

Frequency Response of Nanoelectromechanical Cantilevers Operating in Fluid

Michael J. Martin and Brian H. Houston

Code 7136, Naval Research Laboratory, 4555 Overlook Avenue, Washington, DC, 20375-5320
martinm2@asme.org

Abstract-Nano-electro-mechanical resonators used for sensing, data storage, and nano-fabrication applications are often operated as feed-back control systems. To determine the transfer function of silicon cantilevers with a width of 5.0 μm , a thickness of 800 nm, and lengths of 10, 15, 30, and 45 μm , the damping in air and liquid was simulated numerically using an integrated fluid-structure solver. Bode diagrams and Nyquist plots of the cantilever transfer function indicate that the resonator will behave as a heavily damped system in liquid, and a lightly damped system in air. After experimental validation, this computational method is expected to allow prediction of frequency response prior to fabrication of NEMS resonators.

I. INTRODUCTION

As the applications of cantilever-based nano-systems [1] expand to include chemical sensing [2], medical instrumentation [3], data storage [4], atomic-force microscopy [5], and nano-fabrication [6] the need for sophisticated actuation and control will also increase. [7] This requires determination of the frequency response of the system, which will be heavily influenced by the damping. [8] When cantilevers operate in gas or liquid, the damping of the system is dominated by viscous losses. These losses can be computed using the Navier-Stokes equations on the cantilever cross-section. [9]- [12]

Navier-Stokes solvers have been successfully integrated with simplified structural models to estimate the frequency response of AFM cantilevers in liquid in the low kHz range. [13] The present work uses this computational approach to examine the frequency response of silicon NEMS cantilevers with natural frequencies in the high kHz range vibrating in air and water.

II. COMPUTATIONAL METHOD

The cantilever geometry, with width b , thickness d , and length l , is shown as fig. 1:

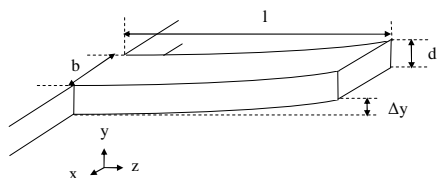


Fig. 1. System Geometry.

The natural frequency of the system ω_n will be given by

$$\omega_n = \frac{f_n}{2\pi} = \left(\frac{k_n}{l} \right)^2 \sqrt{\frac{EI}{m}} \quad (1)$$

where k_n is the vibrational mode constant, E is the Elastic modulus, I is the moment of inertia, and m is the cross-sectional mass. For a cantilever in the first mode of vibration, k_n is equal to 1.875. [14] The cross-sectional mass and the moment of inertia are given by:

$$m = \rho_s b d \quad (2)$$

$$E = b d^3 / 12 \quad (3)$$

where ρ_s is the density of the cantilever.

This geometry can be simplified to the 2-dimensional lumped-parameter model shown in fig. 2. The system consists of a cross-sectional effective mass attached to a spring with effective spring stiffness:

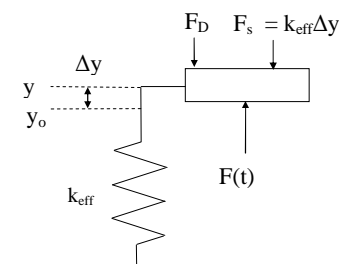


Fig. 2. Lumped-Parameter Model.

The equation of motion is then given by:

$$m \frac{d^2 y}{dt^2} = F(t) - F_D - k_{eff} (y - y_0) \quad (4)$$

where F_D is the viscous drag force, and $F(t)$ is the actuation force. This system will have a natural frequency given by:

$$\omega_n = \sqrt{k_{eff} / m_{eff}} \quad (5)$$

For a thermally actuated cantilever, the actuation force is assumed to be uniformly distributed across the cantilever length. Based on beam theory [15], the effective stiffness is:

$$k_{eff} = 8EI / l^4 \quad (6)$$

Report Documentation Page

Form Approved
OMB No. 0704-0188

Public reporting burden for the collection of information is estimated to average 1 hour per response, including the time for reviewing instructions, searching existing data sources, gathering and maintaining the data needed, and completing and reviewing the collection of information. Send comments regarding this burden estimate or any other aspect of this collection of information, including suggestions for reducing this burden, to Washington Headquarters Services, Directorate for Information Operations and Reports, 1215 Jefferson Davis Highway, Suite 1204, Arlington VA 22202-4302. Respondents should be aware that notwithstanding any other provision of law, no person shall be subject to a penalty for failing to comply with a collection of information if it does not display a currently valid OMB control number.

1. REPORT DATE AUG 2008		2. REPORT TYPE		3. DATES COVERED 00-00-2008 to 00-00-2008	
4. TITLE AND SUBTITLE Frequency Response of Nanoelectromechanical Cantilevers Operating in Fluid				5a. CONTRACT NUMBER	
				5b. GRANT NUMBER	
				5c. PROGRAM ELEMENT NUMBER	
6. AUTHOR(S)				5d. PROJECT NUMBER	
				5e. TASK NUMBER	
				5f. WORK UNIT NUMBER	
7. PERFORMING ORGANIZATION NAME(S) AND ADDRESS(ES) Naval Research Laboratory, Code 7136, 4555 Overlook Avenue, Washington, DC, 20375-5320				8. PERFORMING ORGANIZATION REPORT NUMBER	
9. SPONSORING/MONITORING AGENCY NAME(S) AND ADDRESS(ES)				10. SPONSOR/MONITOR'S ACRONYM(S)	
				11. SPONSOR/MONITOR'S REPORT NUMBER(S)	
12. DISTRIBUTION/AVAILABILITY STATEMENT Approved for public release; distribution unlimited					
13. SUPPLEMENTARY NOTES See also ADM002137. Proceedings of the 2008 IEEE International Conference on Nanotechnology (8th) Held in Arlington, TX on August 18-21, 2008.					
14. ABSTRACT see report					
15. SUBJECT TERMS					
16. SECURITY CLASSIFICATION OF:			17. LIMITATION OF ABSTRACT Same as Report (SAR)	18. NUMBER OF PAGES 4	19a. NAME OF RESPONSIBLE PERSON
a. REPORT unclassified	b. ABSTRACT unclassified	c. THIS PAGE unclassified			

The effective mass of the system is obtained by Rayleigh's method of setting the natural frequency of the lumped parameter oscillator given in (5) equal to the natural frequency of the cantilever given in (1). [16]

$$m_{eff} = 8m/k_n^4. \quad (7)$$

The actuation force is given by a sinusoid with magnitude F_o and frequency ω :

$$F(t) = F_o \sin(\omega t). \quad (8)$$

The viscous drag force is computed by solving the time-dependent Navier-Stokes equations on a 100 by 120 mesh around the cantilever, using a marker-and-cell CFD code. [17] The complete computational procedure is given by:

1. Solution of the velocity and pressure using a time-dependent Navier-Stokes algorithm.
2. Computation of the fluid force, spring force, and actuation force on the cantilever.
3. Computation of the acceleration, velocity, and position of the cantilever
4. Updating of fluid boundary conditions based on the new cantilever cross-section velocity.

The system time step is set by the maximum allowable time step for the fluid solver. The system achieves equilibrium within 5 to 10 cycles. For each cycle, the maximum displacement, and the phase difference between the maximum displacement and the maximum force are recorded.

III. RESULTS

A. Maximum Displacement

The frequency response of three silicon cantilevers was simulated. All cantilevers simulated have a width of 5 μm and a thickness of 800 nm. The cantilever lengths were 10, 15, 30, and 45 μm . These cantilevers dimensions are of the same order as those proposed for integration into nano-electro-mechanical systems for bio-detection. [1], [18] The elastic modulus used was 160 GPa, and the density was 2400 kg/m^3 . [19] This yields natural frequencies of 6.63×10^7 , 2.95×10^7 , 7.36×10^6 , and $3.27 \times 10^5 \text{ s}^{-1}$.

The cantilever damping was simulated using two fluids: water at 293 K, and air at 103 kPa and 293 K. For water, this corresponds to a density ρ_f of 999.4 kg/m^3 , and a viscosity μ of $1.007 \times 10^{-3} \text{ kg/m-s}$. For air, this corresponds to a density ρ_f of 1.22 kg/m^3 , and a viscosity μ of $1.81 \times 10^{-5} \text{ kg/m-s}$. [20]

Because of the small scale of the system, a slip boundary condition was used in the CFD computation, with a momentum accommodation coefficient of 0.85. [21] This incorporates the continuum break-down effects encountered in nano-systems at atmospheric pressure. For the given cantilevers, the system was swept using a force with magnitude F_o of 10 $\mu\text{N/m}$, with values of ω/ω_n ranging from 0.10 to 7.0 in liquid, and 0.5 to 5.0 in air.

B. Simulation results for cantilevers in water

The peak displacement versus frequency is shown in fig. 3. These results show that the simulation predicts displacements in the nm range, indicating that the physical parameters chosen for the simulation are physically realistic.

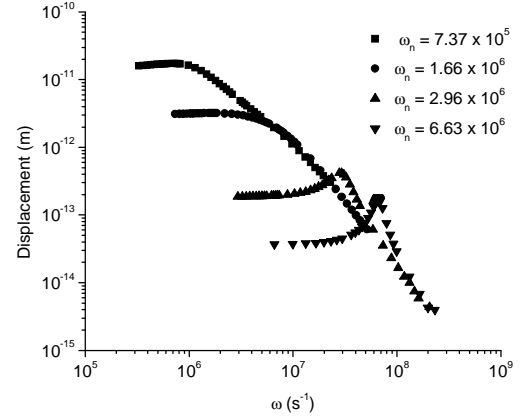


Fig. 3. Displacement versus Frequency for Cantilevers in Liquid.

The displacement results can be normalized to obtain the system gain using (9):

$$G(\omega) = 20 \cdot \log_{10}(k_{eff} y_{max} / F_o). \quad (9)$$

A plot of the gain as a function of the normalized frequency ω/ω_n is shown as fig. 4:

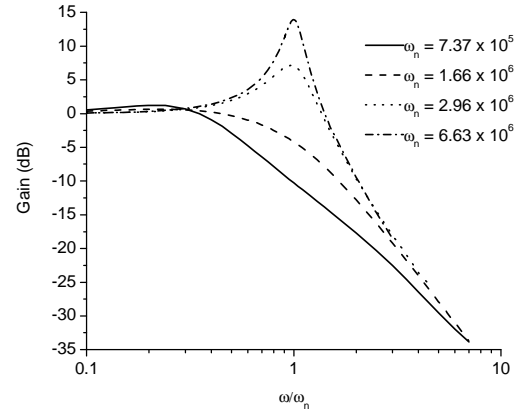


Fig. 4. Gain versus Frequency for Cantilevers in Liquid.

Fig. 4 shows that the cantilever operating in liquid is a heavily damped system, with a large shift in the resonant frequency away from the natural frequency of the system. This is confirmed by computing the quality factor of the system, as shown in table (1). The quality factors of less than one are similar to previous experimental results for long cantilever resonators in liquid. [5]

Table (1) shows a large gain the quality factor as the resonator natural frequency increases. This is consistent with previous experience operating cantilevers at higher frequencies [5] and higher-order modes. [22] These results show that the quality factor is proportional to the natural frequency of the system raised to the 1.4, which suggests that the damping is frequency dependent.

TABLE I

RESONANT FREQUENCY AND QUALITY FACTORS FOR CANTILVERS IN LIQUID

Natural Frequency f_n (MHz)	Natural Frequency ω_n (s^{-1})	Resonant Frequency ω_r (s^{-1})	ω_r/ω_n	Q
10.6	6.63×10^7	6.62×10^7	0.9985	10.15
4.69	2.94×10^7	2.85×10^7	0.969	4.56
1.17	7.37×10^6	1.67×10^6	0.226	0.58
0.521	3.74×10^6	7.88×10^5	0.211	0.23

A plot of the phase difference between the peak force and the peak displacement is shown as fig. 5. Together, fig. 4 and fig. 5 constitute the Bode plots of the resonators when operating in liquid.

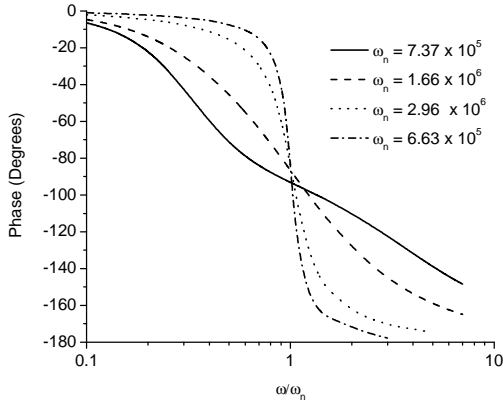


Fig. 5. Phase versus Frequency for Cantilevers in Liquid.

The data in fig. 4 and fig. 5 can be used to prepare the Nyquist diagram of the system. This result, shown in fig. 6, can be used to evaluate the stability of proposed control algorithms for the system.

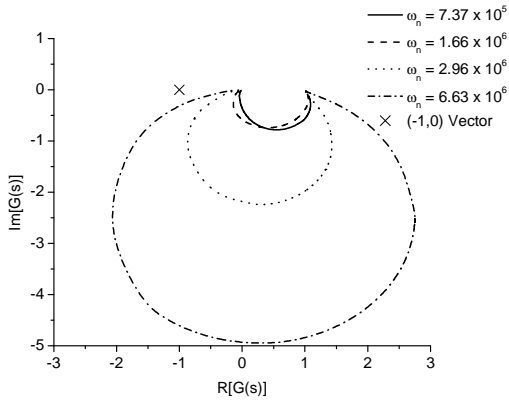


Fig. 6. Nyquist Diagram for Cantilevers in Liquid.

C. Simulation results for cantilevers in air

The analysis performed for the resonators using water as a working fluid is repeated using air as a working fluid. The maximum resonator displacements obtained through numeric simulation are shown as fig. 7:

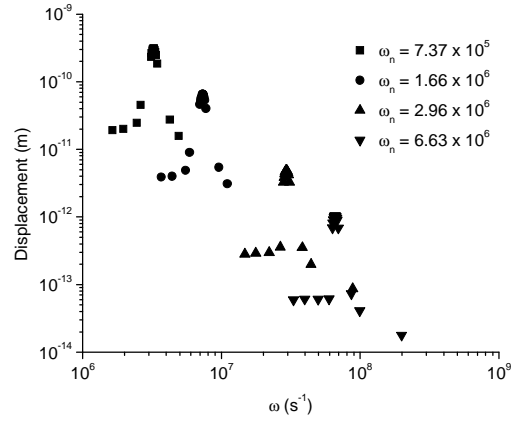


Fig. 7. Displacement versus Frequency for Cantilevers in Air.

These results can be used to obtain the gain, as shown in fig. 8:

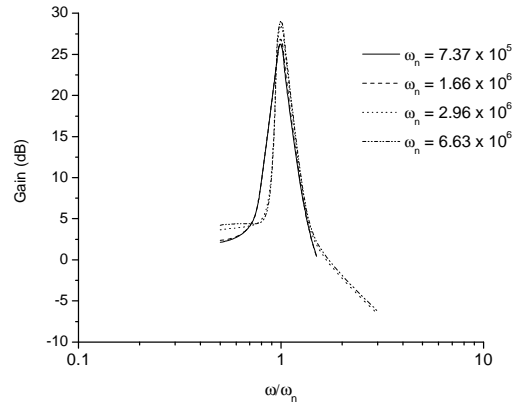


Fig. 8. Gain versus Frequency for Cantilevers in Air.

The frequency shifts and the quality factor obtained are shown in table (2). The quality factors in air are typically orders of magnitude higher than the estimated quality factors in water for the same resonator, which agrees with experimental results. [4], [23]

TABLE II

RESONANT FREQUENCY AND QUALITY FACTORS FOR CANTILVERS IN AIR

Natural Frequency f_n (MHz)	Natural Frequency ω_n (s^{-1})	Resonant Frequency ω_r (s^{-1})	ω_r/ω_n	Q
10.6	6.63×10^7	6.62×10^7	0.9992	19.9
4.69	2.94×10^7	2.93×10^7	0.9985	15.8
1.17	7.37×10^6	7.32×10^6	0.9937	10.8
0.521	3.74×10^6	3.71×10^6	0.9916	10.4

These results show that the quality factor is proportional to the natural frequency of the system raised to the 0.23, again indicating frequency-dependent damping. However, the relative resolution of this technique for determining quality factor is less than other techniques that compute Q directly by computing the energy loss at resonance. [12]

A plot of the phase difference between the peak force and the peak displacement is shown as fig. 9. Together, fig. 8 and fig. 9 constitute the Bode plots of the resonators when operating in air.

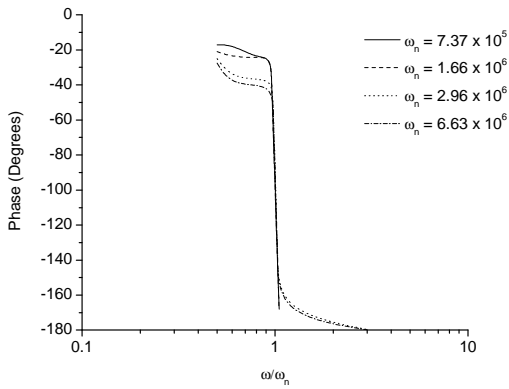


Fig. 9. Phase versus Frequency for Cantilevers in Air.

The large computational cost of performing simulations of cantilevers vibrating in air prevented reconstruction of the entire Nyquist diagram. Selected points of the Nyquist diagram for the system operating in air are shown as fig. 10:

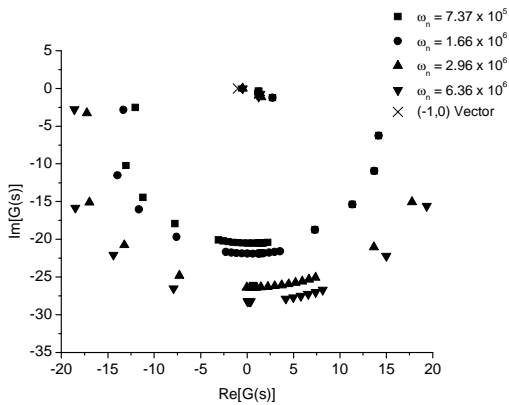


Fig. 10. Nyquist Diagram for Cantilevers in Air.

IV. CONCLUSIONS

For cantilevers operating in air, the frequency response is relatively unaffected by the natural frequency of the system. For cantilevers in water, there is a large difference in the frequency response at higher frequencies, due to increased damping. However, the high computational cost of simulating resonators operating in air limited comparisons off behavior away from the resonance frequency.

These results predict the dynamic response and the frequency shift from resonance without use of empirical expressions such as added mass. If the results for the frequency response are experimentally validated, then capturing the dynamic response by simulation will allow optimization of NEMS for integration with feed-back control without trial-and-error experimental design.

ACKNOWLEDGMENT

The authors acknowledge financial support from the Office of Naval Research. Simulations were performed using the facilities of the Army Research Laboratory Major Shared

Resource Center, an initiative of the DOD High Performance Computing Modernization Program.

REFERENCES

- [1] M. Li, H. X. Tang, and M. Roukes, "Ultra-sensitive NEMS-based cantilevers for sensing, scanned probe and very high-frequency applications," *Nature Nanotechnology*, vol. 2, pp. 114-120, 2007.
- [2] N. V. Lavrik, M. J. Sepaniak, and P. G. Datskos, "Cantilever transducers as a platform for chemical and biological sensors," *Review of Scientific Instruments*, vol. 75, pp. 2229-2253, 2004.
- [3] Y. Zhao, S. Li, A. Davidson, B. Yang, Q. Wang, and Q. Lin, "A MEMS viscometric sensor for continuous glucose monitoring," *Journal of Micromechanics and Microengineering*, vol. 17, pp. 2528-2537, 2007.
- [4] P. Vettiger, G. Cross, M. Despont, U. Drechsler, U. Durig, B. Gotsmann, W. Haberle, M. A. Lantz, H. E. Rothuizen, R. Stutz, and G. K. Binnig, "The "millipede"-nanotechnology entering data storage," *IEEE Transactions on Nanotechnology*, vol. 1, pp. 39-54, 2002.
- [5] D. A. Walters, J. P. Cleveland, N. H. Thomson, P. K. Hansma, M. A. Wendman, G. Gurley, and V. Elings, "Short cantilevers for atomic force microscopy," *Review of Scientific Instruments*, vol. 67, pp. 3583-3590, 1996.
- [6] R. D. Piner, J. Zhu, F. Xu, S. Hong, and C. A. Mirkin, "Dip-pen nanolithography," *Science*, vol. 283, pp. 661-663, 1999.
- [7] F. J. Rubio-Sierra, R. Vazquez, and R. W. Stark, "Transfer Function Analysis of the Micro Cantilever Used in Atomic Force Microscopy," *IEEE Transactions on Nanotechnology*, vol. 6, pp. 692-700, 2006.
- [8] G. F. Franklin, J. D. Powell, and A. Emani-Naiedi, *Feedback Control of Dynamic Systems*. Upper Saddle River, NJ: Prentice Hall, 2002.
- [9] F. R. Blom, S. Bouwstra, M. Elwenspoek, and J. H. J. Fluitman, "Dependence of the quality factor of micromachined beam resonators on pressure and geometry," *Journal of Vacuum Science and Technology, Series B*, vol. 10, pp. 19-26, 1992.
- [10] R. B. Bhiladvala and Z. J. Wang, "Effect of fluids on the Q factor and resonance frequency of oscillating micrometer and nanometer beams," *Physical Review E*, vol. 69, 036307, 2004.
- [11] J. E. Sadler, "Frequency response of cantilever beams immersed in viscous fluids with applications to the atomic force microscope," *Journal of Applied Physics*, vol. 84, pp. 64-76, 1998.
- [12] M. J. Martin and B. H. Houston, "Computation of Damping for Vibrating Micro-Machined Cantilevers in the Slip Flow Regime," AIAA Paper 2008-0690 (2008)
- [13] M. J. Martin, H. K. Fathy and B. H. Houston, "Dynamic simulation of atomic force microscope cantilevers oscillating in liquid," *J. of Applied Physics*, submitted
- [14] W. Weaver, S. P. Timoshenko, and D. H. Young, *Vibration Problems in Engineering*. New York: John Wiley and Sons, 1990
- [15] W. C. Young and R. Bydinas, *Roark's Formulas for Stress and Strain*, New York, NY: McGraw-Hill Professional, 2001.
- [16] W. T. Thomson, *Theory of Vibration with Application*, Englewood Cliffs, NJ: Prentice Hall, 1993.
- [17] F. H. Harlow, and J. E. Welch, "Numerical Calculation of Time-Dependent Viscous Incompressible Flow of Fluid with Free Surface," *Physics of Fluids*, Vol. 8, pp. 2182-2189, 1965.
- [18] K. L. Aubin, J. Huang, S.-M. Park, Y. Yang, M. Kondratovich, H. G. Craighead, and B. R. Ilic, "Microfluidic encapsulated nanoelectromechanical resonators," *Journal of Vacuum Science and Technology B*, vol. 25, pp. 1171-11, 2007.
- [19] N. Maluf, *An Introduction to Microelectromechanical Systems Engineering*. Boston, MA: Artech House Publishing, 2000.
- [20] F. P. Incropera and D. P. DeWitt, *Fundamentals of Heat and Mass Transfer*. New York, NY: John Wiley & Sons, 1990.
- [21] E. B. Arkilic, M. A. Schmidt, and K. S. Breuer, "Gaseous slip flow in long microchannels," *Journal of MicroElectroMechanical Systems*, vol. 6, pp. 167-178, 1997.
- [22] M. K. Ghatkesar, T. Braun, V. Barwich, J.-P. Ramseyer, C. Gerber, M. Hegner, and H. P. Lang, "Resonating modes of vibrating microcantilevers in liquid," *Applied Physics Letters* vol. 92, pp. 043106-1-3, 2008.
- [23] J. F. Vignola, J. A. Judge, J. Jarzynski, M. Zalalutdinov, B. H. Houston, and J. A. Baldwin, "Effect of viscous loss on mechanical resonators designed for mass detection," *Applied Physics Letters* vol. 88, pp. 041921-1-3, 2006.